nature COMMUNICATIONS

ARTICLE

https://doi.org/10.1038/s41467-019-09504-3 OPEN

Anion-adaptive crystalline cationic material for $^{99}TcO_4^-$ trapping

Lei Mei[1], Fei-ze Li[1], Jian-hui Lan[1], Cong-zhi Wang[1], Chao Xu[2], Hao Deng[1], Qun-yan Wu[1], Kong-qiu Hu[1], Lin Wang[1], Zhi-fang Chai[1,3], Jing Chen[2], John K. Gibson[4] & Wei-qun Shi[1]

Efficient anion recognition is of great significance for radioactive $^{99}TcO_4^-$ decontamination, but it remains a challenge for traditional sorbents. Herein, we put forward a tactic using soft crystalline cationic material with anion-adaptive dynamics for $^{99}TcO_4^-$ sequestration. A cucurbit[8]uril-based supramolecular metal-organic material is produced through a multi-component assembly strategy and used as a sorbent for effective trapping of TcO_4^-. Excellent separation of TcO_4^-/ReO_4^- is demonstrated by fast removal kinetics, good sorption capacity and high distribution coefficient. Remarkably, the most superior selectivity among metal-organic materials reported so far, together with good hydrolytic stability, indicates potential for efficient TcO_4^- removal. The structure incorporating ReO_4^- reveals that the supramolecular framework undergoes adaptive reconstruction facilitating the effective accommodation of TcO_4^-/ReO_4^-. The results highlight opportunities for development of soft anion-adaptive sorbents for highly selective anion decontamination.

[1] Laboratory of Nuclear Energy Chemistry, Institute of High Energy Physics, Chinese Academy of Sciences, Beijing 100049, China. [2] Nuclear Chemistry and Chemical Engineering Division, Institute of Nuclear and New Energy Technology, Tsinghua University, Beijing 100084, China. [3] Engineering Laboratory of Nuclear Energy Materials, Ningbo Institute of Industrial Technology, Chinese Academy of Sciences, Ningbo, Zhejiang 315201, China. [4] Chemical Sciences Division, Lawrence Berkeley National Laboratory, Berkeley, California 94720, USA. These authors contribute equally: Lei Mei, Fei-ze Li, Jian-hui Lan. Correspondence and requests for materials should be addressed to W.-q.S. (email: shiwq@ihep.ac.cn)

^{99}Tc, a long-lived ($t_{1/2} = 2.13 \times 10^5$ y) radioisotope of technetium, is an abundant and problematic nuclear waste component and potent radioactive pollution source[1,2]. Complex chemical behavior of ^{99}Tc hampers separation of uranium and plutonium during reprocessing of spent nuclear fuel, and high volatility of ^{99}Tc species (Tc_2O_7) constrains incorporation into glass waste forms via high-temperature vitrification. ^{99}Tc, as a stable TcO_4^- in its dominant + 7 oxidation state, is highly water soluble and can migrate readily in the environment, thereby posing severe environmental risks. Therefore, efficient capture of radioactive ^{99}Tc has received considerable attention for both nuclear waste management and contaminant remediation purposes.

Solvent extraction and ion exchange are two well-established effective methods for removal of TcO_4^- from aqueous media[3–6]. In solvent extraction, extractants with anion recognition capability can achieve high selectivity for TcO_4^- [4,7–9], but practical applications are limited by cost and inefficiency. Ion exchange is developed as an alternative of traditional extraction. Despite the ease of implementation and the expected efficient recovery of TcO_4^- based on ion-exchange method[5,10], the total performance of sorbent materials used seems not to be competent. For example, most traditional polymeric materials exhibit slow anion exchange kinetics and poor radiation resistance[11,12], while inorganic cationic materials such as layered double hydroxide (LDH)[13], sulfides[14], and borates[15,16] exhibit low sorption capacity and poor selectivity. The emergence of hydrolytically stable cationic metal–organic materials (MOMs) has led to potent applications for capture of oxyanion pollutants[3,17–20]. High porosity, structural diversity, and functional tunability[21–23] render these hybrid materials as promising candidates for TcO_4^- removal[24,25]. However, there is still demand for improvement in terms of selectivity of TcO_4^- sorbents, with enhanced discrimination for TcO_4^-/ReO_4^- over other anions as a particularly desirable attribute.

There is no doubt that anion receptors[7,9,26–29] of TcO_4^- have the best ion selectivity. A rational approach for improving the selectivity of solid sorbents is to give sorbent materials an ideal ion-recognition capability by direct functionalization of traditional solid sorbents with covalently attached anion receptors (Fig. 1a)[30,31], but unfortunately, chemical modification method generally suffers from the necessity for elaborate syntheses and possible deactivation of functional recognition groups after implanting in bulk materials. Herein, inspired by molecular recognition of anion receptors, we put forward an alternative tactic that circumvents this drawback via an easily prepared anion-adaptive sorbent material that can behave like an anion receptor itself (Fig. 1b)[32–36]. Conceptually, this soft sorbent material is capable of dynamically tuning the structural arrangement of its framework in response to different anions, enabling attainment of an optimized pore size and shape match for maximum interactions with, and the resulting selectivity for target anions such as TcO_4^-. Specifically, the desirable anion-adaptive sorbent material should have two crucial attributes of structural dynamics and anion-responsive capability, which can be easily achieved in self-organization-based supramolecular materials bearing recognition sites[37,38]. Glycoluril derivatives containing abundant –CH or $–CH_2$ motifs as potent anion-recognition sites, among which *endo*-type bambusurils can serve as anion receptors[39–41], while *exo*-type cucurbiturils exhibit anion-binding affinity through outer-surface interaction (Fig. 1c), can be used to prepare a class of anion-adaptive cationic materials for specific anion removal[42–45]. A multicomponent assembly strategy is proposed for synthesizing such sorbents based on a versatile glycoluril-based macrocyclic host, cucurbit[8]uril (CB8). The CB8 macrocycle used here plays a vital role in accomplishing both the construction of a supramolecular network[46–48] and anion recognition (Fig. 1d), and endows both important attributes mentioned above: (a) abundant CH and CH_2 groups on its waist for outer-surface hydrogen-bonding recognition to promote the TcO_4^- capture; (b) flexibility of the CB8 encapsulation motif allowing dynamics of the overall supramolecular framework[49–51].

In this work, a CB8-based cationic supramolecular metal–organic framework, SCP-IHEP-1 ($[Cu((bpy)_2@CB8)(H_2O)_4](NO_3)_2{\cdot}18H_2O$), is constructed by the supramolecular collaborative assembly. As expected, this material is demonstrated to be an efficient and selective sorbent capable of reversibly sequestrating TcO_4^-/ReO_4^- by trapping them in specific tetrahedral pores created by CB8 moieties arranged in order. The anion-adaptive capability of this supramolecular sorbent toward effective TcO_4^- recognition resembles the dynamic behavior of the receptor during ion recognition, and can be taken as a representative TcO_4^--specific smart sorbent material.

Results

Assembly of SCP-IHEP-1 based on CB8. The cationic supramolecular framework material, SCP-IHEP-1, was synthesized via assembly of CB8, 4,4′-bipyridine (bpy) and $Cu(NO_3)_2$ under hydrothermal conditions. It crystallizes in monoclinic space group $P2_1/n$ (Supplementary Table 1) as pale blue block crystals (Supplementary Figure 1). Crystal structure of SCP-IHEP-1 reveals that all the four components (CB8, bpy, Cu^{2+}, and NO_3^-) (Supplementary Figure 2) are included during the self-assembly process, and the main building unit of the supramolecular framework of SCP-IHEP-1 (Fig. 2a) is a one-dimensional (1D) metal–organic polyrotaxane chain (Fig. 2b) based on encapsulation motif, 2bpy@CB8, linked by Cu^{2+} (Fig. 1c). Given the potential for competition between metal coordination and supramolecular encapsulation of bpy, one-pot synthesis of SCP-IHEP-1 having both types of connectivities for bpy suggests stepwise assembly, with initial supramolecular encapsulation of bpy in CB8 followed by assembly into a 1D chain via bpy-Cu^{2+} coordination (Supplementary Figure 3). This assembly mechanism was corroborated by an alternative two-step method in which isolation of the dimeric bpy units encapsulated in CB8, 2bpy@CB8, in the form of $[(bpy)_2@CB8]_{0.5}{\cdot}[(bpy)_2@CB8]_{0.5}{\cdot}19H_2O$ (Supplementary Figure 4 and 5) is followed by assembly with the metal ions provided as $Cu(NO_3)_2$. It is notable that, whereas 2G@H encapsulation, where G denotes a guest molecule, and H a host, is common for host CB8[46–48,52], this motif is rare for neutral guest such as bpy in CB8[53]. Actually, formation of 2bpy@CB8 in aqueous solution involves a large favorable enthalpy change as a result of release of high-energy water (Supplementary Figure 6 and Supplementary Table 2), which should be taken as the main driving force for this encapsulation[54,55] and results in different degrees of pi–pi stacking (Supplementary Figure 4) and a variety of hydrogen bonds between CB8 and bpy (Supplementary Figure 7 and Supplementary Table 3).

Cationic 1D polyrotaxane chains in SCP-IHEP-1 can further assemble into a three-dimensional (3D) supramolecular framework via cross-linkage of a large number of interchain hydrogen bonds (Supplementary Figure 8 and Supplementary Table 4). The nitrate counterions are located in tetrahedral cavities formed by four neighboring CB8 from the 1D chains (Fig. 2d, e and Supplementary Figure 9), and also contributed a lot to the formation of final supramolecular framework via anion-directed assembly (Fig. 2f). Analysis of the local nitrate anion environment reveals its interaction with only two CB8 macrocycles of the tetrahedral cavity through a limited number of hydrogen bonds (Supplementary Figure 10), suggesting weak interaction with

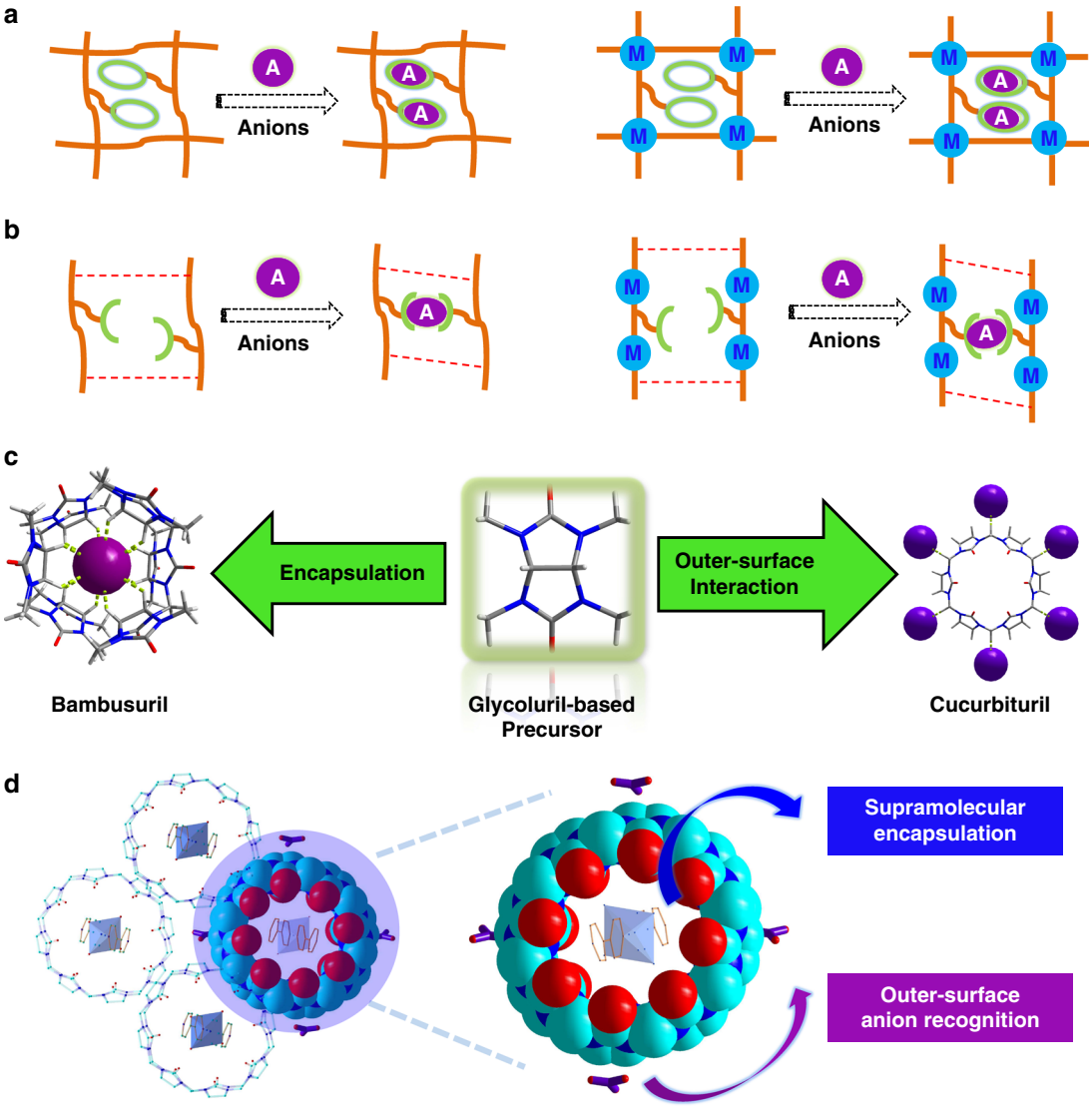

Fig. 1 Design strategies for introducing anion-adaptive capability to sorbent materials. **a** Direct modification of organic polymers or metal–organic sorbents with macrocyclic motifs bearing anion-recognition ability (orange lines: backbones of solid sorbents; green circles: anion receptors; purple balls marked as "A": anions; blue balls marked as "M": metal nodes). **b** Supramolecular assembly of smart polymers or metal–organic sorbents exhibiting anion-adaptive behaviors (orange lines: backbones of solid sorbents; green curves: anion-recognition sites; purple circles: anions; blue balls: metal nodes). **c** Glycoluril-based macrocyclic hosts for anion recognition through two different modes (purple balls: anions). **d** Dual roles of CB8 in accomplishing both the construction of a supramolecular network by encapsulation and providing outer-surface interaction sites for anion recognition: left, a full view of CB8-based supramolecular framework; right: enlarged diagram of CB8 showing its interactions with the surrounding components (red balls: O atoms; light-blue balls: C atom; dark blue balls: N atoms)

main 1D backbones of SCP-IHEP-1 and the potential for exchange with oxyanions having more favorable interactions, such as TcO_4^-/ReO_4^-.

In contrast, coordination assembly simply from bpy and Cu $(NO_3)_2$ in the absence of CB8 macrocycles results in a twofold interpenetrating 3D framework based on six-coordinated copper nodes with deformed octahedral geometry (namely as Cu-bpy, see Supplementary Table 1 and Supplementary Figure 11). In addition to the nitrate directly binding to a copper center, there should be a disordered nitrate anion in the pore of 3D framework to balance the charge.

After exposure of SCP-IHEP-1 crystals for 12 h at 298 K to aqueous solutions with pH values ranging from 3 to 11, the structure as determined by powder X-ray diffraction (PXRD) remained essentially unchanged (Fig. 3a). The results suggest thermal and hydrolytic stability, despite the flexible supramolecular framework. Meanwhile, in contrast to significant dehydration of Cu-bpy at low temperatures (Supplementary Figure 12), SCP-IHEP-1 did not undergo any significant decomposition until over 205 °C (Fig. 3b), suggesting its high thermal stability.

Sorption performance for ReO_4^- removal. ReO_4^- was initially used as a nonradioactive structural analog of $^{99}TcO_4^-$ to assess anion exchange of SCP-IHEP-1. Batch kinetics experiment shows that removal of ReO_4^- by SCP-IHEP-1 follows the pseudo-first-order model (Supplementary Figure 13 and Supplementary Table 5), and is achieved to 88% removal at 1 min and to over 95% after 10 min (Fig. 4a). The fast kinetics of ReO_4^- exchange by SCP-IHEP-1 is superior to those of other cationic metal–organic materials such as SLUG-21[20], UiO-66-NH_3^+[17],

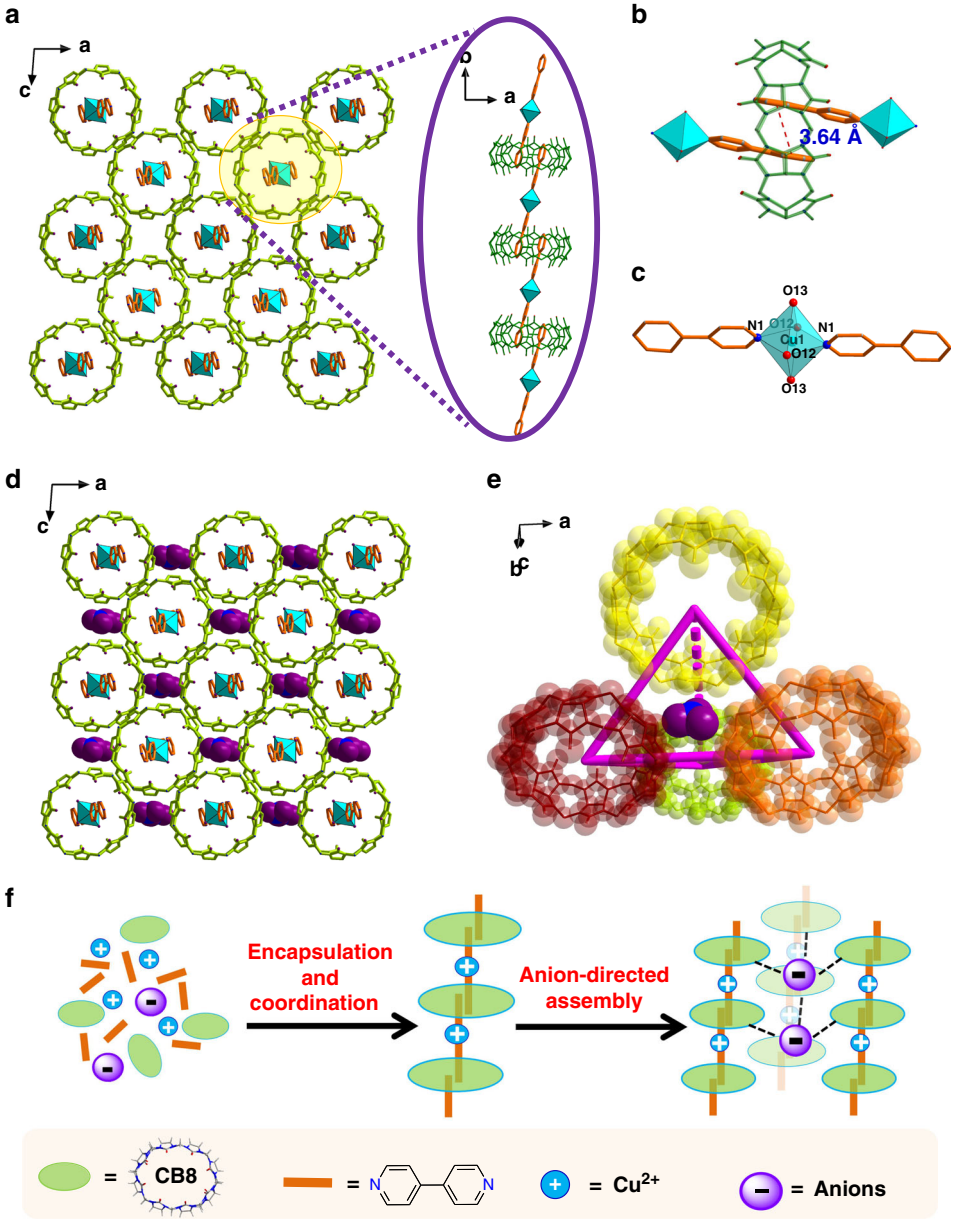

Fig. 2 Crystal structure of SCP-IHEP-1. **a** The cationic supramolecular framework (insert: building blocks of the 1D metal–organic polyrotaxane chain, green macrocycles: cucurbit[8]uril (CB8) molecules; skeletons in orange: 4,4′-bipyridine (bpy); polyhedra in mint green: coordination spheres of copper ion; **b** the supramolecular assembly motif of 2bpy@CB8; **c** $[Cu(bpy)_2(H_2O)_4]^{2+}$ coordination motif; **d** nitrate-incorporated supramolecular framework of SCP-IHEP-1 (purple: O atom; blue: N atom); **e** NO_3^- in a tetrahedral coordination cavity; **f** proposed stepwise self-assembly process of SCP-IHEP-1 involving four different components

and Ni(II)-based MOF[19], all of which take over 24 h to reach exchange equilibrium for sequestering ReO_4^-. It is notably that, SCP-IHEP-1 also shows faster removal rate and much higher removal ratio than its CB8-free counterpart Cu-bpy (an equilibrium time of 30 min and a final removal ratio of 20%, Supplementary Figure 14 and Supplementary Table 6).

As revealed by the sorption isotherm experiment (Fig. 4b), the calculated maximum sorption capacity of SCP-IHEP-1 based on the Langmuir model is 157 mg Re g^{-1} sorbent corresponding to 211 mg ReO_4^- g^{-1} sorbent (Supplementary Figure 15 and Supplementary Table 7), which is higher than those for LDH (130 mg ReO_4^- g^{-1})[13], NDTB-1 (49 mg ReO_4^- g^{-1})[15,]16, and UiO-66-NH_3^+ (159 mg ReO_4^- g^{-1})[17]. Assuming that all the nitrate ions can be exchanged, the sorption capacity of SCP-IHEP-1 for ReO_4^- observed here reaches to as high as 93% of the theoretical value (226 mg g^{-1}), suggesting its nearly perfect exchange tendency for ReO_4^-. Moreover, the distribution coefficient (K_d) of SCP-IHEP-1 toward ReO_4^- is 2.6×10^5 mL g^{-1} (Supplementary Table 8), which is also comparable to recently emerging high-performance cationic MOFs, SCU-100, and SCU-101 (Table 1)[24,25], and ensures the decontamination depth of ReO_4^-. In contrast, ReO_4^- removal by CB8-free Cu-bpy can only achieve a poor separation efficiency (K_d: ~1×10^3 mL g^{-1}, Supplementary Table 8), which is two orders of magnitude lower than that of SCP-IHEP-1. Correspondingly, the derived maximum sorption capacity of 138 mg ReO_4^- g^{-1} (Supplementary Figure 16 and Supplementary Table 9) only reaches 14%

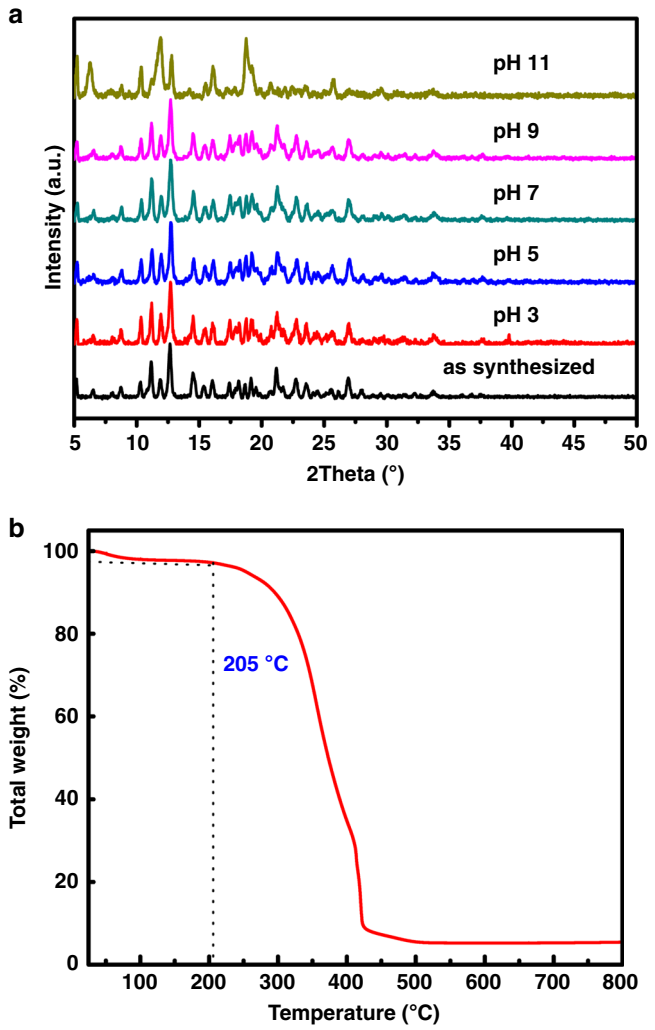

Fig. 3 Hydrolytic stability and thermal stability of SCP-IHEP-1. **a** PXRD patterns of SCP-IHEP-1 after soaking in aqueous solutions with varying pH values ranging from 3 to 11 for 12 hours at 298 K. **b** Thermogravimetric analysis (TGA) in air for SCP-IHEP-1

of the theoretical value (950 mg ReO_4^- g^{-1} assuming all the anions could be exchangeable.

In terms of structural reversibility, over 96% of sorbed ReO_4^- could be exchanged with NO_3^- in a desorption solution of 0.5 M $NaNO_3$, and the regenerated material retains over 92% of removal percentage after two cycles. The removal percentage of SCP-IHEP-1 for ReO_4^- keeps at a high level (>96%) within a wide pH range of 4−10 (Fig. 4c) and remains up to 60% at more acidic media with a pH value of 2, revealing a good hydrolytic stability and high separation capability. Studies on the effect of temperature (Supplementary Figure 17) indicates that the present anion exchange may be an exothermic process with an enthalpy change of −25.76 kJ mol^{-1} (Supplementary Table 10).

Uptake selectivity. Studies on ReO_4^- exchange selectivity show that SCP-IHEP-1 still selectively removes ReO_4^- in the presence of one equivalent of several competing anions including NO_3^-, SO_4^{2-}, CO_3^{2-}, PO_4^{3-}, or ClO_4^- (Fig. 4d). Although ReO_4^- removal diminishes somewhat when competing with structurally similar ClO_4^-, it remains as high as 91% (Supplementary Table 11). Under similar conditions, ReO_4^- removal by SCU-101[24] does not exceed 90%, and removal by PAF-1-F[56] is only ca. 20% in the presence of SO_4^{2-} or PO_4^{3-}.

Given the high concentration of nitrate ion in high level nuclear waste stream, the competing effect of excess nitrate anions is critical during TcO_4^- removal. Moreover, for certain types of nuclear waste, high-concentration SO_4^{2-} is also another potent competing anions. Therefore, ReO_4^- removal with higher concentrations of competing NO_3^- and SO_4^{2-} were further studied to check the uptake selectivity of ReO_4^-. As shown in Fig. 3e, removal of ReO_4^- remains as high as 96% for a molar ratio of NO_3^- to ReO_4^- of 20:1, and is 84% for a ratio of 100:1 (Supplementary Table 12). Remarkably, an increase in SO_4^{2-} has little effect on the uptake of ReO_4^- (Fig. 3f), with removal falling only from 98 to 92% when the SO_4^{2-}:ReO_4^- ratio increases from 1:1 to 4000:1 (Supplementary Table 13).

Removal selectivity of SCP-IHEP-1 toward TcO_4^-/ReO_4^- can be partially ascribed to its inherent feature of inorganic–organic hybrid material based on multi-component collaborative assembly. Generally, anions with higher charge density such as SO_4^{2-} often have better uptake than those with lower charge density (TcO_4^-/ReO_4^-) during the sorption process with inorganic anion sorbents[13,15,16]. However, this order always is reversed for organic polymers and inorganic–organic hybrid materials, which is taken as a Hofmeister phenomenon[57]. This Hofmeister behavior might be originated from the hydrophobic nature of organic backbones of these materials, as evidenced by the methylene/methylidyne-rich tetrahedral pores of SCP-IHEP-1.[3] A similar trend is observed for other MOMs bearing local hydrophobic cavities or pores[24,25,58]. That is to say, considering the differences in hydration energy of anions, the preference for larger poorly hydrated ReO_4^- anions over NO_3^- or SO_4^{2-} reflects the important role of hydration/dehydration in the anion exchange, which is consistent with the exothermic feature of exchange observed above.

TcO_4^- removal from simulated nuclear wastes. The overall selectivity of SCP-IHEP-1 toward ReO_4^- against NO_3^- and SO_4^{2-} observed here is better than those of MOF-typed (SCU-101)[25] and polymeric network-typed (SCU-CPN-1)[57] anionic exchange materials with excellent ReO_4^-/TcO_4^- removal performance emerging recently, making it a promising candidate for selective sequestration of TcO_4^- from waste solutions, even in the presence of high concentration of competing anions. To assess the potential application of SCP-IHEP-1 in real nuclear solutions containing radioactive TcO_4^-, removal experiments for TcO_4^- were also tested. Uptake kinetics of TcO_4^- by SCP-IHEP-1 is as fast as that of ReO_4^-, achieving ~80% removal at 1 min and over 90% after 10 min (Fig. 5), and nearly quantitative removal after 2 h. In a simplified simulated waste stream containing 9.8 ppm $^{99}TcO_4^-$ in 0.03 M HNO_3 (i.e., a NO_3^- concentration ~ 500 times higher than TcO_4^-), although the TcO_4^- removal is affected by the high-concentration competing NO_3^-, the removal percentage of TcO_4^- is still up to 79.2% using a solid-to-liquid ratio (SLR) of 0.5, which is superior to the removal by SCU-100 (59.3% with a SLR of 1.0)[25] and SCU-101 (75.2% with a higher SLR of 10)[24] and represents the best removal performance for $^{99}TcO_4^-$ among cationic MOMs reported so far.

Mechanism for selective ReO_4^- uptake. ReO_4^- (and by inference TcO_4^-) exchange of SCP-IHEP-1 was monitored by Fourier transform infrared spectroscopy (FTIR) (Fig. 6a), PXRD patterns (Fig. 6b), and energy dispersive X-ray spectroscopy (EDS) (Fig. 6c). Single crystals of ReO_4^- incorporated material (SCP-IHEP-1-Re) were also obtained and subject to X-ray diffraction structural determination on the Beijing Synchrotron Radiation

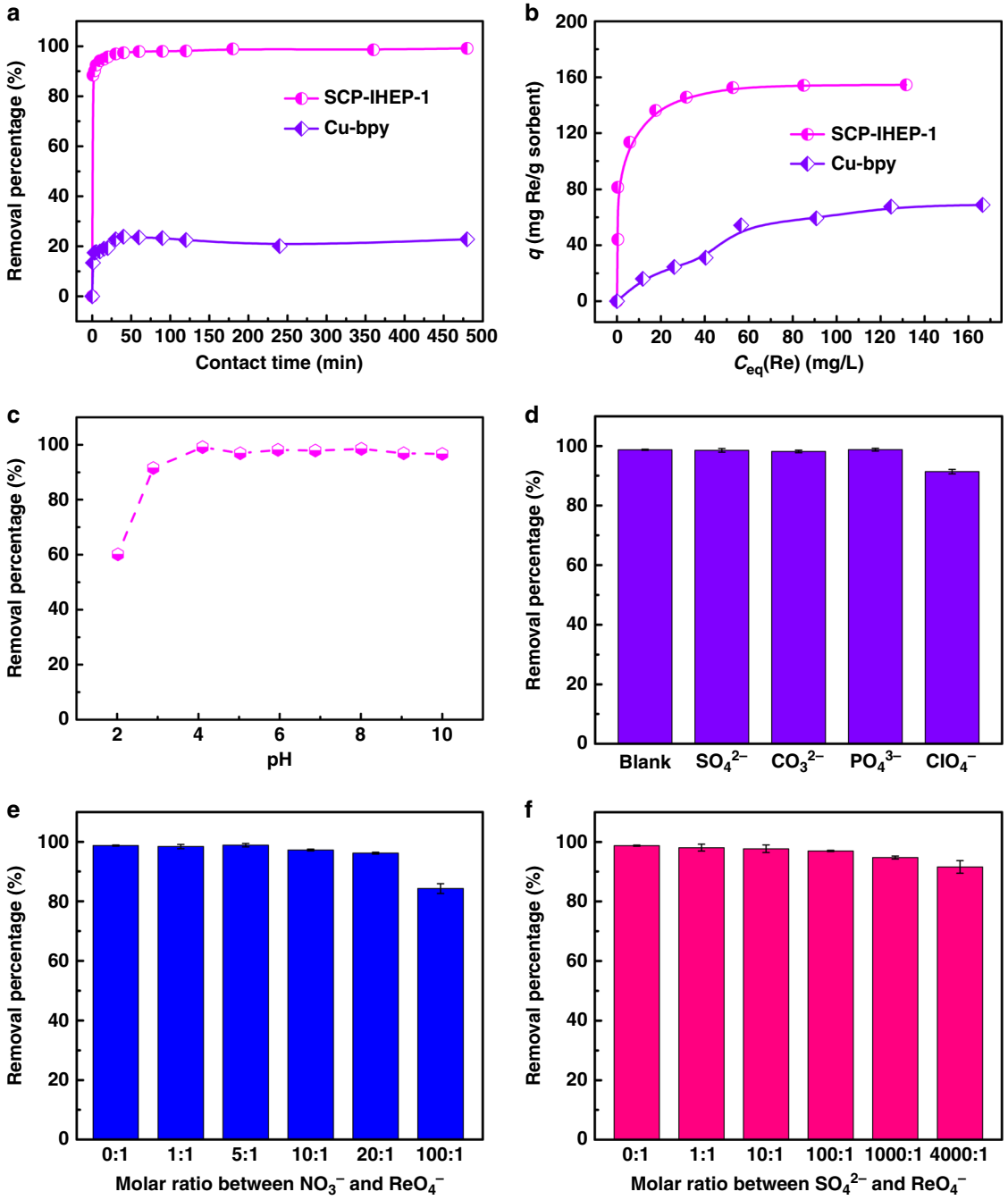

Fig. 4 Performance of SCP-IHEP-1 for ReO_4^- removal. **a** Sorption kinetics with that of Cu-bpy used as a comparison; **b** sorption isotherms with that of Cu-bpy used as a comparison; **c** effect of pH on the removal percentage of ReO_4^- ($c_0 = 44.6$ mg L^{-1}, $T = 300$ K, $t = 12$ h, $V = 8$ mL, and $m = 4$ mg); **d** effect of competing anions on the ReO_4^- exchange ($c_0 = 45.0$ mg L^{-1}, $t = 12$ h, $T = 300$ K, $V = 8$ mL, $m = 4$ mg, and pH = 6.92); **e** effect of excess NO_3^- on the ReO_4^- exchange ($c_0 = 45.0$ mg L^{-1}, $t = 12$ h, $T = 300$ K, $V = 8$ mL, $m = 4$ mg, and pH = 6.85); **f** effect of excess SO_4^{2-} on the ReO_4^- exchange ($c_0 = 45.0$ mg L^{-1}, $t = 12$ h, $T = 300$ K, $V = 8$ mL, $m = 4$ mg, and pH = 7.05). Error bars represent the s.d. of uncertainty for each point

Facility (BSRF) (Supplementary Figure 18). A comparison of simulated PXRD pattern of crystalline SCP-IHEP-1-Re and actual PXRD of SCP-IHEP-1 after ReO_4^- exchange (Supplementary Figure 19) confirms that they are totally identical to each other, and crystallographic analysis at the molecular level will be very helpful to understand the recognition mechanism of SCP-IHEP-1 toward ReO_4^- as well as TcO_4^-. Similarly, ReO_4^- uptake of Cu-bpy was also evidenced by the signals of ReO_4^- or Re in FTIR (Supplementary Figure 20) and EDS (Supplementary Figure 21) after exchange experiments. PXRD comparison (Supplementary Figure 22) between Cu-bpy after ReO_4^- exchange and ReO_4^- incorporated crystalline analog of Cu-bpy (Supplementary Figure 23) suggests a possible ReO_4^--induced transformation of Cu-bpy to Cu-bpy-Re along with significant change of Cu^{2+} coordination sphere and total topological structure, although there might be also a small amount of other undefined products.

Analysis on the crystal structure of SCP-IHEP-1-Re reveals that ReO_4^- is trapped in tetrahedral pores surrounded by four adjacent CB8 molecules (Fig. 6d) and fixed by a mass of hydrogen

Table 1 Comparison of ReO_4^- removal performance between different cationic materials

Materials	K_d (mL g^{-1})	Removal rate (ReO_4^--NO_3^-) (%)	Removal rate (ReO_4^--SO_4^{2-}) (%)	Removal rate (ReO_4^--PO_4^{3-}) (%)	Removal rate (ReO_4^--ClO_4^-) (%)	Ref.
LDH	262	-	-	-	-	25
NDTB-1	652	-	-	-	-	25
PAF-1-F	2.55×10^5		19	21	-	56
UiO-66-NH_3^+	-	-	50	15	21	17
SCU-100	3.3×10^5	-	98.5	98.7	-	25
SCU-101	7.5×10^5	91.7	85.6	89.2	87.2	24
SCP-IHEP-1	2.6×10^5	98.4	98.5	98.8	91.4	This work

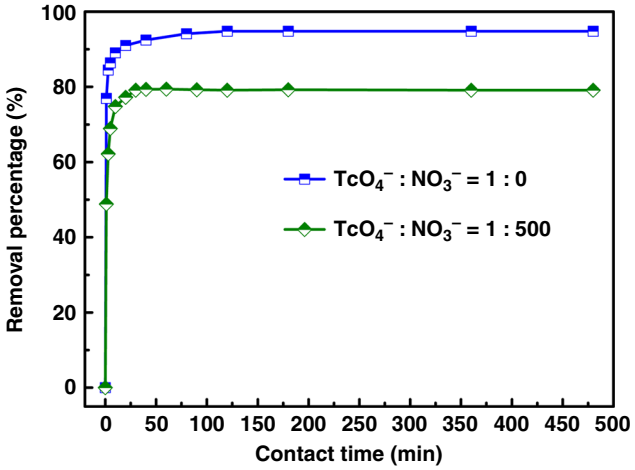

Fig. 5 Removal of TcO_4^- as a function of contact time in the absence of competing anion NO_3^- (blue line; TcO_4^-: NO_3^- = 1: 0, c_0 = 10 mg L^{-1}, V = 40 mL, m = 20 mg, and pH = 7.00) and in the presence of 0.03 M NO_3^- (green line; TcO_4^-: NO_3^- = 1: 500, c_0 = 10 mg L^{-1}, V = 10 mL, m = 5 mg, and pH = 6.89). Error bars represent the s.d. of uncertainty for each point

bonds between anion oxygen atoms and outer-surface CH and CH_2 groups (a total of 15 such bonds with an average O·H distance of 2.71 Å) (Supplementary Table 3). The crystal structure of SCP-IHEP-1-Re reveals close-packing mode similar to SCP-IHEP-1 but with a change of stacking orientation originated from its single-crystal-to-single-crystal (SCSC) transformation upon ReO_4^- incorporation (Fig. 7a). Compared to the coordination environment of NO_3^- in SCP-IHEP-1, encapsulation of ReO_4^- is achieved by the rearrangement of surrounding CB8 moieties with a resulting slight deformation of the tetrahedral pores (Fig. 7b). The above results indicate that the removal of TcO_4^-/ReO_4^- by SCP-IHEP-1 is mainly attributed to anion-adaptive reorganization of the CB8-based pores, which can dynamically adapt to the encapsulated anionic guest.

A comparison of this CB8-based MOM sorbent material with Cu-bpy or other CB8-free MOM sorbents material such as SLUG-21[20,41] and SBN[58] reveals that the removal of TcO_4^-/ReO_4^- by SCP-IHEP-1 leads to little structural change of supramolecular framework, while anion removal by the latter ones rely on coordination of target anions with metal centers accompanied by irreversible significant structural arrangement (Supplementary Figure 24). Evidently, the inherent flexibility of soft supramolecular framework of SCP-IHEP-1 facilitates a fast dynamic recognition process, and thus enables superior kinetics as well as good reversibility of anion exchange. Especially, the involvement of CB8 macrocycles in SCP-IHEP-1 plays a vital role in directing supramolecular assembly process, and can be indeed an important contributor to high selectivity in terms of constructing ordered pores for anion trapping and interacting with trapped anions through a mass of hydrogen bonds. The fast kinetics, reversibility and selectivity as well as high efficiency by this type of soft supramolecular material make it outcompetes with traditional cationic MOM sorbents.

In order to understand the driving force underlying the specific ReO_4^-/TcO_4^- uptake, theoretical calculation methods were used to analyze the interactions of CB8-based host cationic framework with different anions (NO_3^-, ReO_4^-, and TcO_4^-) within SCP-IHEP-1 or SCP-IHEP-1-Re. The GGA-PBE[59] functional implemented in VASP 5.4[60] was used to optimize the unit cells of the crystals, allowing relaxation of all the atom coordinates. With the fully optimized unit cells, three anion-containing tetrahedral pore models based on a simplified host system [**H**] consisting of the key components of the CB8 macrocycles were built (Supplementary Figure 25). Electrostatic potential (ESP) distribution analysis of these simplified models shows that, the portal carbonyls of CB8 exhibit negative ESP, while the waist CH_2/CH groups exhibit positive ESP that facilitates interaction with negative-charged moieties such as NO_3^- and ReO_4^- (Supplementary Figure 26 and Supplementary Table 14). Besides the ESP maps, hydrogen bonding orbital interaction analysis from the MO perspective were also studied, and the results reveal that orbital interactions contribute to several hydrogen bonds as evidenced by that of [**H**] and ReO_4^- (Supplementary Figure 27).

To further clarify hydrogen bonding interactions between CB8-based host [**H**] and anions, quantum theory of atoms in molecules (QTAIM) analysis was performed at the B3LYP-D3 (BJ)/6-311+G(d,p) level of theory (see Supplementary Methods for details). Several bond critical points (BCPs) between [**H**] and oxygen atoms of NO_3^- and ReO_4^- can be observed (Supplementary Figure 28), indicating noncovalent interactions between CB8-based host [**H**] and these anions. The parameters of electron density (ρ), Laplacian of electron density ($\nabla^2\rho$), kinetic energy density (G), and potential energy density (V) at the representative BCPs are listed in Supplementary Table 15. These values are in the range $0.02 < \rho < 0.07$ e/Å^3, $0.2 < \nabla^2\rho < 0.8$ e/Å^5, $4.5 < G < 18.3$ kJ/mol/Bohr^3, $-15.7 < V < -3.1$ kJ/mol/Bohr^3, respectively. For shorter H-Bond lengths (e.g., 2.511 Å), these values are within the scope of weak hydrogen bonding, while the larger ones belong to van der Waals interactions[61–63]. These intermolecular interactions can be further detected by independent gradient model (IGM)[64] analysis and reduced density gradient (RDG)[65] analysis (Fig. 8 and Supplementary Figure 29 and 30), and proved be weak hydrogen bonding (light-blue area in isosurfaces) and van der Waals interactions (green area in isosurfaces). The results are in excellent agreement with the QTAIM analysis. Besides, the low-density and

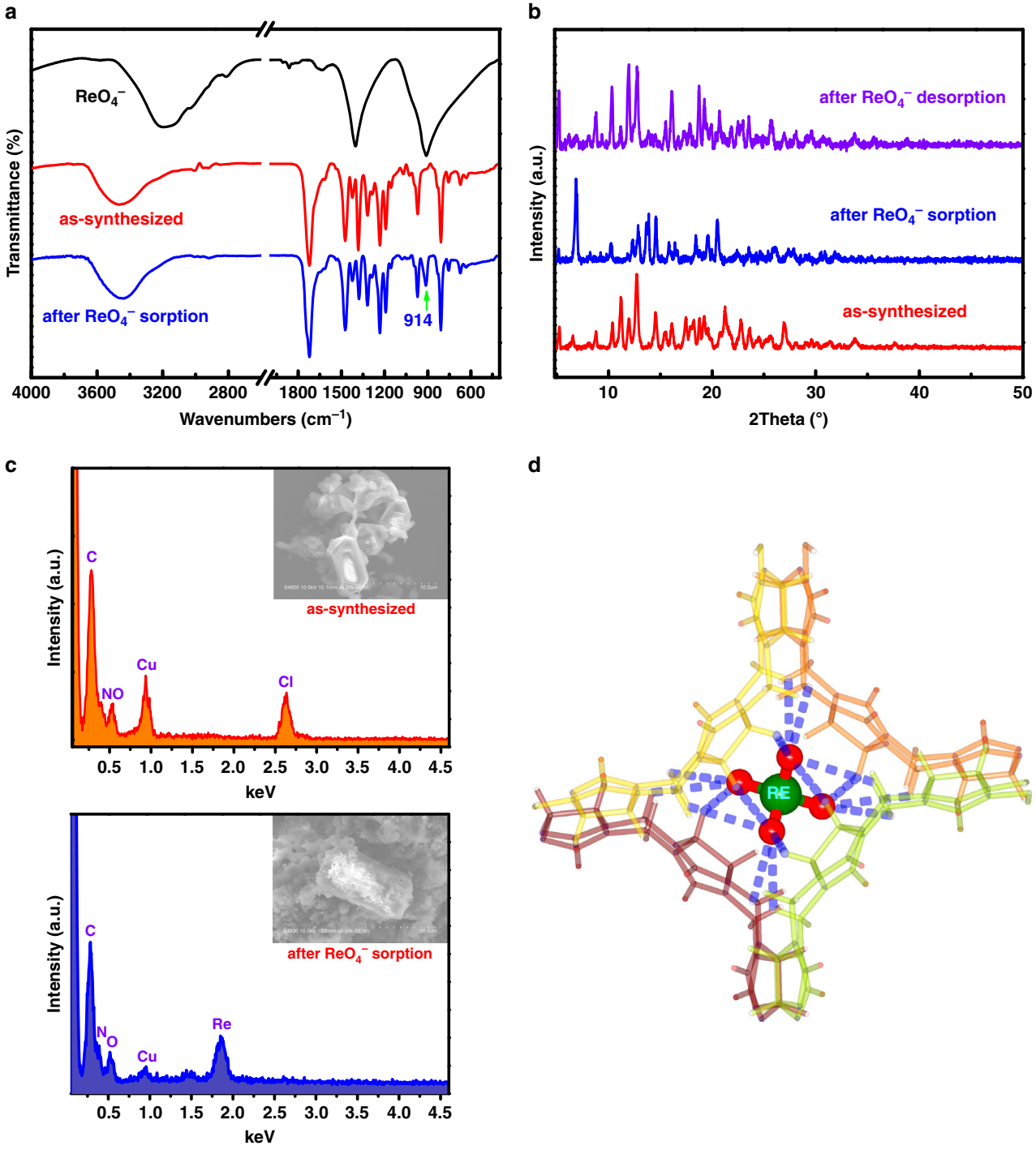

Fig. 6 Characterization of SCP-IHEP-1 after ReO_4^- sorption. **a** IR spectra of SCP-IHEP-1 before (red) and after (blue) ReO_4^- exchange; **b** PXRD patterns before ReO_4^- sorption (red), after ReO_4^- sorption (blue) and after material recovery by ReO_4^- desorption in a solution of 0.5 M $NaNO_3$ (purple); **c** EDS of SCP-IHEP-1 before (top) and after (bottom) ReO_4^- exchange; **d** ReO_4^- instead of NO_3^- trapped in a tetrahedral coordination cavity after ReO_4^- sorption (four adjacent CB8 molecules are shown in different colors and hydrogen atoms in black)

low-gradient spikes of RDG analysis also confirm the presence of noncovalent interactions (Supplementary Figure 31). In all, the calculation results suggest the vital role of hydrogen bonds in stabilizing the [**H**]-anion inclusion motifs and thus facilitating the effective accommodation of target anions in the flexible cationic supramolecular framework.

We computed hydration energies, binding energies and total energies for anion exchange with [**H**] based on anion-containing tetrahedral pore models built as above (see Supplementary Figure 32). The computed total energies (BE_{aq}) are similar for TcO_4^- and ReO_4^-, and both of them are larger than that of NO_3^--[**H**] model (Supplementary Table 16). Further energy analysis shows that difference of anion-[**H**] binding energies (ΔBE_{gas}) for all these three models are not significant, whilst the difference of hydration energy (ΔE_{hyd}) between ReO_4^- and NO_3^- is dominant. This result suggests the vital role of hydrophobic nature of

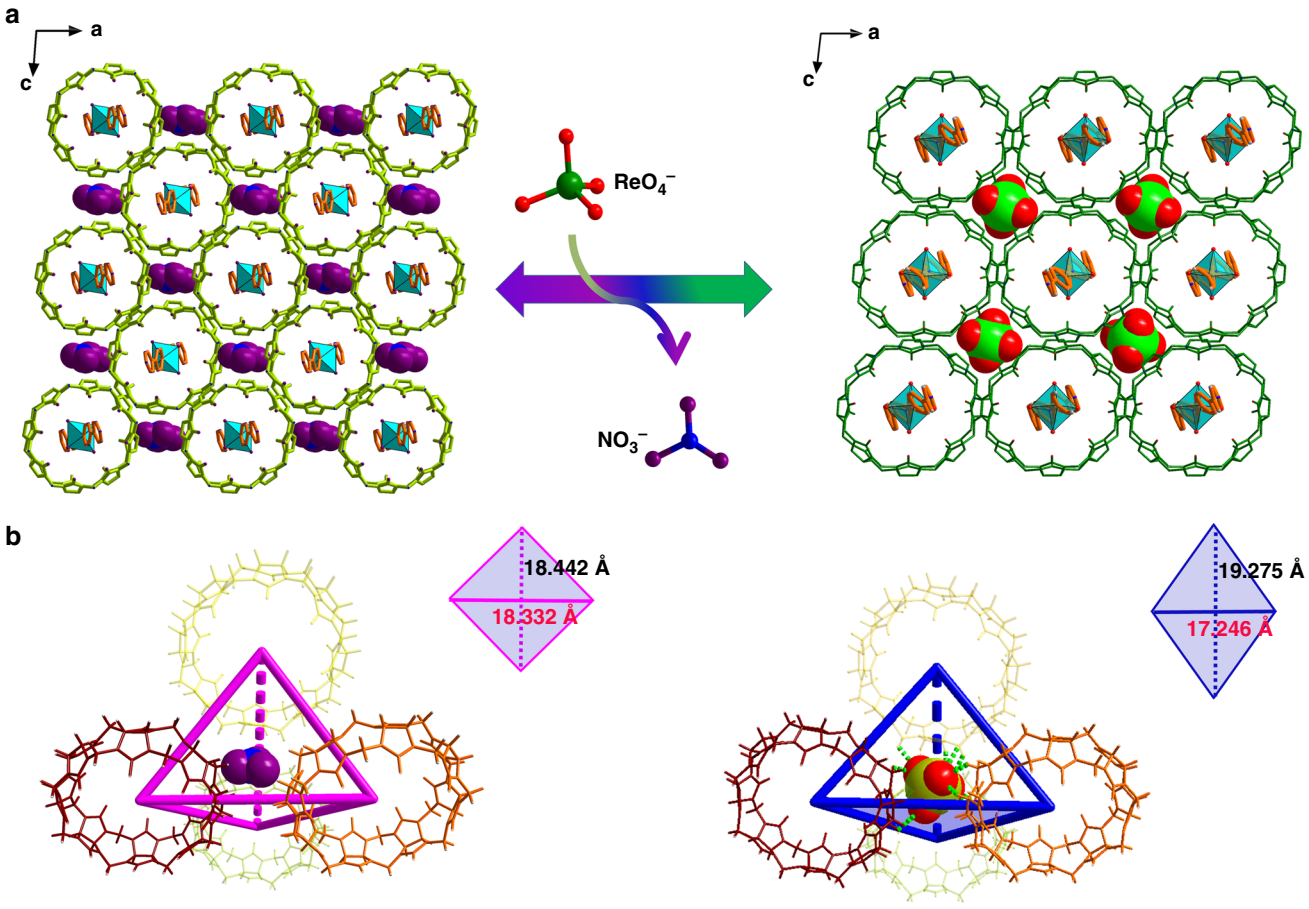

Fig. 7 ReO_4^- exchange-triggered structural transformation of SCP-IHEP-1. **a** Single-crystal-to-single-crystal (SCSC) transformation from SCP-IHEP-1 to SCP-IHEP-1-Re upon ReO_4^- incorporation. **b** Adaptive structural transformation of CB8-based tetrahedral cavity after encapsulation of ReO_4^-

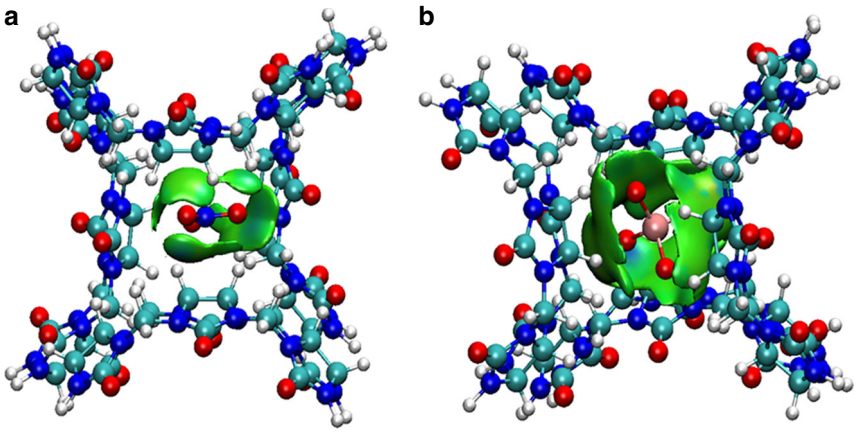

Fig. 8 Intermolecular interactions (isosurfaces: 0.005 a.u.) for different models using IGM analysis. **a** CB8-based host [**H**] and NO_3^-; **b** CB8-based host [**H**] and ReO_4^- (blue represents a strong attraction, and red denotes a strong repulsion). All isosurfaces are colored according to a BGR (blue-green-red) scheme over the electron density range $-0.05 < \mathrm{sign}(\lambda_2)\rho < 0.05$ a.u

CB8-based methylene/methylidyne-rich tetrahedral pores of SCP-IHEP-1 in selective TcO_4^-/ReO_4^- removal, and thus provides a valuable evidence for the Hofmeister bias selectivity of SCP-IHEP-1 mentioned before.

Discussion

We put forward a tactic using anion-adaptive cationic material with structural dynamics for $^{99}TcO_4^-$ sequestration. As a conceptual prototype, a soft supramolecular material, SCP-IHEP-1, was synthesized and has been demonstrated to exhibit excellent removal performance of TcO_4^- (and ReO_4^-), especially in selectivity against competing anions. This exceptional performance is attributed to the anion-adaptive rearrangement of the CB8-surrounded pores, which can adapt to the encapsulated anionic guest. Hydration energy difference between displaced NO_3^- and target oxoanions should be the essential driving

force for facilitating selective TcO_4^- uptake of sorbents with hydrophobic pores. The result suggests the potential of this anion-adaptive cationic material SCP-IHEP-1 for effective TcO_4^- removal, and most importantly, paves a way for developing high efficiency sorbents for anion removal based on soft sorbent materials with anion-adaptive dynamics and efficient anion recognition capability to achieve selective and specific anion binding.

Methods

Materials. Caution! Tc-99 possesses significant health risks when inhaled or digested and should be handled according to standard precautions and procedures. All Tc-99 studies were conducted in a licensed laboratory dedicated to radiological investigations. Cucurbit[8]uril (CB8) was synthesized according to the previously-reported literature[66]. 4,4′-bipyridine (bpy), $Cu(NO_3)_2$, NH_4ReO_4, and other reagents were analytically pure and used as received. $^{99}TcO_4^-$ stock solutions were prepared by dissolving certain amounts of NH_4TcO_4 (99%) in deionized water or NO_3^- solution as desired.

One-pot synthesis of SCP-IHEP-1. An aliquot of 0.2 M $Cu(NO_3)_2$ aqueous solution (200 μL, 0.04 mmol) was added to a suspension of 4,4′-bipyridine (bpy) (0.006 g, 0.04 mmol) and CB8 (0.026 g, 0.02 mmol) in water (2 mL) in a stainless-steel vessel. The mixture was sealed, and kept at 150 °C for 48 h. After cooling to room temperature, the obtained blue microcrystals of SCP-IHEP-1 were filtered, rinsed with water and ethanol three times, and dried in air at room temperature. Yield: 0.026 g (59% based on CB8).

Two-step synthesis of SCP-IHEP-1. (a) 2bpy@CB8: 4,4′-bipyridine (bpy) (0.006 g, 0.04 mmol) was added to a suspension of CB8 (0.026 g, 0.02 mmol) in water (2 mL). After incubation in a stainless-steel vessel at 150 °C for 24 h, colorless block crystals of 2bpy@CB8 were obtained in a quantitative yield during cooling to room temperature. The structure of 2bpy@CB8 was confirmed by single-crystal structure determination as $[(bpy)_2@CB8]_{0.5}\cdot[(bpy)_2@CB8]_{0.5}\cdot 19H_2O$ (Figure S4) and ^{1}H-NMR spectra (Figure S5). ^{1}H NMR (500 MHz, D_2O, δ ppm): 8.49 (m, 8H); 7.42 (m, 8H), 5.84 (d, 16H), 5.52 (s, 16H), 4.22 (d, 16H). (b) SCP-IHEP-1: 0.2 M $Cu(NO_3)_2$ aqueous solution (500 μL, 0.04 mmol) was added to a suspension of 2bpy@CB8 intermediate obtained as described above in water (2 mL) in a stainless-steel vessel. The mixture was sealed, and kept at 150 °C for 48 h. After cooling to room temperature, light-blue block crystals of SCP-IHEP-1 were obtained in a high yield (~0.045 g, >99%).

Synthesis of Cu-bpy. An aliquot of 0.2 M $Cu(NO_3)_2$ aqueous solution (500 μL, 0.10 mmol) was added to a suspension of 4,4′-bipyridine (bpy) (0.016 g, 0.10 mmol) in water (1.5 mL) in a stainless-steel vessel. The mixture was sealed, and heated slowly to 150 °C in a period of 24 h, and kept at 150 °C for another 48 h. After slowly cooling to room temperature in a period of 24 h, the obtained blue regular plate-like crystals of Cu-bpy were filtered, rinsed with water three times, and dried in air at room temperature. Yield: 0.013 g.

Synthesis of SCP-IHEP-1-Re. To elucidate the exchange and recognition mechanism for SCP-IHEP-1 with ReO_4^- (and by inference TcO_4^-), crystals of ReO_4^--incorporated SCP-IHEP-1 sorbent were synthesized through an in situ assembly method. The detailed synthesis procedure is as follows: 0.2 M $Cu(NO_3)_2$ aqueous solution (200 μL, 0.04 mmol) and 0.2 M NH_4ReO_4 aqueous solution (400 μL, 0.04 mmol) was added to a suspension of 2bpy@CB8 obtained as described above in water (2 mL) in a stainless-steel vessel. The mixture was sealed, and kept at 150 °C for 48 h. After cooling to room temperature, small light-blue prismatic crystals of SCP-IHEP-1-Re were obtained. The PXRD pattern of SCP-IHEP-1 after ReO_4^- uptake collected is fully consistent with the simulated PXRD pattern based on crystal data for SCP-IHEP-1-Re obtained above, suggesting identical structures.

Synthesis of Cu-bpy-Re. An aliquot of 0.2 M $Cu(NO_3)_2$ aqueous solution (500 μL, 0.10 mmol) and 0.2 M NH_4ReO_4 aqueous solution (400 μL, 0.04 mmol) was added to a suspension of 4,4′-bipyridine (bpy) (0.006 g, 0.04 mmol) in water (2.0 mL) in a stainless-steel vessel. The mixture was sealed, and heated slowly to 150 °C in a period of 24 h, and kept at 150 °C for another 48 h. Blue block crystals of Cu-bpy-Re were obtained after slowly cooling to room temperature in a period of 24 h.

X-ray single-crystal structure determination. X-ray diffraction data for SCP-IHEP-1, Cu-bpy, and Cu-bpy-Re were acquired on a Bruker D8 VENTURE X-ray CMOS diffractometer with a Cu Kα X-ray source ($\lambda = 1.54178$ Å) at room temperature. Data frames were collected using the program APEX 3 and processed using the program SAINT routine in APEX 3. Data collection for 2bpy@CB8 and SCP-IHEP-1-Re was acquired with synchrotron radiation at Beijing Synchrotron Radiation Facility (BSRF, $\lambda = 0.72$ Å) using a MAR CCD detector. The crystal was mounted in nylon loops and cooled in a cold nitrogen-gas stream at 100 K. Data were indexed, integrated and scaled using DENZO and SCALEPACK from the HKL program suite. All crystal structures were solved by means of direct methods and refined with full-matrix least squares on SHELXL-97[67], and refined with full-matrix least squares on SHELXL-2014[67,68]. The crystal data of all compounds are given in Supplementary Table 1.

Batch experiments. All the sorption experiments were conducted using the batch sorption method. The solid/liquid ratio performed in all batch experiments was 0.5 g L^{-1}. In a typical experiment, 4 mg of SCP-IHEP-1 or Cu-bpy was added into 8 mL of aqueous solution with a certain concentration of ReO_4^-. The pH values of the solutions were adjusted as required using NaOH and HNO_3 and were measured on a digital pH-meter. The mixture was stirred for a specified time (t, min) at a specified temperature (T, K), and separated with a 0.22 μm nylon membrane filter. The concentrations of ReO_4^- in aqueous solution were determined by inductively coupled plasma optical emission spectrometry (ICP-OES, Horiba JY2000-2).

Data availability

Details for measurements and characterization, detailed experimental procedures, computational methods are given in the Supplementary Methods. The X-ray crystallographic coordinates for structures reported in this study have been deposited in the Cambridge Crystallographic Data Center under accession numbers CCDC: 1874188 (2bpy@CB8), 1874189 (SCP-IHEP-1), 1874190 (SCP-IHEP-1-Re), 1894900 (Cu-bpy), and 1894899 (Cu-bpy-Re), respectively. These data can be obtained free of charge via http://www.ccdc.cam.ac.uk/data_request/cif). All data are either provided in the Article and its Supplementary Information or available from the corresponding author upon request.

Received: 19 November 2018 Accepted: 12 March 2019
Published online: 04 April 2019

References

1. Darab, J. G. & Smith, P. A. Chemistry of technetium and rhenium species during low-level radioactive waste vitrification. *Chem. Mater.* **8**, 1004–1021 (1996).
2. Popova, Ny. N. et al. Technetium: behaviour during reprocessing of spent nuclear fuel and in environmental objects. *Russ. Chem. Rev.* **72**, 101–121 (2003).
3. Custelcean, R. & Moyer, B. A. Anion separation with metal-organic frameworks. *Eur. J. Inorg. Chem.* **2007**, 1321–1340 (2007).
4. Katayev, E. A., Kolesnikov, G. V. & Sessler, J. L. Molecular recognition of pertechnetate and perrhenate. *Chem. Soc. Rev.* **38**, 1572–1586 (2009).
5. Wilmarth, W. R. et al. Review: waste-pretreatment technologies for remediation of legacy defense nuclear wastes. *Solvent Extr. Ion. Exch.* **29**, 1–48 (2011).
6. Banerjee, D., Kim, D., Schweiger, M. J., Kruger, A. A. & Thallapally, P. K. Removal of TcO_4^- ions from solution: materials and future outlook. *Chem. Soc. Rev.* **45**, 2724–2739 (2016).
7. Alberto, R., Bergamaschi, G., Braband, H., Fox, T. & Amendola, V. $^{99}TcO_4^-$: selective recognition and trapping in aqueous solution. *Angew. Chem. Int. Ed.* **51**, 9772–9776 (2012).
8. Kubik, S. Anion recognition in aqueous media by cyclopeptides and other synthetic receptors. *Acc. Chem. Res.* **50**, 2870–2878 (2017).
9. Zhang, D. W., Ronson, T. K., Mosquera, J., Martinez, A. & Nitschke, J. R. Selective anion extraction and recovery using a (Fe_4L_4)-L-II cage. *Angew. Chem. Int. Ed.* **57**, 3717–3721 (2018).
10. Burgeson, I. E., Deschane, J. R. & Blanchard, D. L. Removal of technetium from Hanford tank waste supernates. *Sep. Sci. Technol.* **40**, 201–223 (2005).
11. Davenas, J. et al. Stability of polymers under ionising radiation: the many faces of radiation interactions with polymers. *Nucl. Instrum. Meth. B* **191**, 653–661 (2002).
12. Derradji, M. et al. Toward advanced gamma rays radiation resistance and shielding efficiency with phthalonitrile resins and composites. *Nucl. Instrum. Meth. B* **421**, 13–17 (2018).
13. Wang, Y. F. & Gao, H. Z. Compositional and structural control on anion sorption capability of layered double hydroxides (LDHs). *J. Colloid Interface Sci.* **301**, 19–26 (2006).
14. Neeway, J. J. et al. Removal of TcO_4^- from representative nuclear waste streams with layered potassium metal sulfide materials. *Chem. Mater.* **28**, 3976–3983 (2016).
15. Wang, S. A. et al. NDTB-1: a supertetrahedral cationic framework that removes TcO_4^- from solution. *Angew. Chem. Int. Ed.* **49**, 1057–1060 (2010).

16. Wang, S. A. et al. Selectivity, kinetics, and efficiency of reversible anion exchange with TcO_4^- in a supertetrahedral cationic framework. *Adv. Funct. Mater.* **22**, 2241–2250 (2012).
17. Banerjee, D. et al. Zirconium-based metal-organic framework for removal of perrhenate from water. *Inorg. Chem.* **55**, 8241–8243 (2016).
18. Colinas, I. R., Silva, R. C. & Oliver, S. R. J. Reversible, selective trapping of perchlorate from water in record capacity by a cationic metal-organic framework. *Environ. Sci. Technol.* **50**, 1949–1954 (2016).
19. Desai, A. V., Manna, B., Karmakar, A., Sahu, A. & Ghosh, S. K. A water-stable cationic metal-organic framework as a dual adsorbent of oxoanion pollutants. *Angew. Chem. Int. Ed.* **55**, 7811–7815 (2016).
20. Fei, H. H., Bresler, M. R. & Oliver, S. R. J. A new paradigm for anion trapping in high capacity and selectivity: crystal-to-crystal transformation of cationic materials. *J. Am. Chem. Soc.* **133**, 11110–11113 (2011).
21. Eddaoudi, M. et al. Modular chemistry: secondary building units as a basis for the design of highly porous and robust metal-organic carboxylate frameworks. *Acc. Chem. Res.* **34**, 319–330 (2001).
22. Furukawa, H., Cordova, K. E., O'Keeffe, M. & Yaghi, O. M. The chemistry and applications of metal-organic frameworks. *Science* **341**, 974–988 (2013).
23. Li, J. R., Sculley, J. & Zhou, H. C. Metal-organic frameworks for separations. *Chem. Rev.* **112**, 869–932 (2012).
24. Zhu, L. et al. Identifying the recognition site for selective trapping of $^{99}TcO_4^-$ in a hydrolytically stable and radiation resistant cationic metal-organic framework. *J. Am. Chem. Soc.* **139**, 14873–14876 (2017).
25. Sheng, D. P. et al. Efficient and selective uptake of TcO_4^- by a cationic metal-organic framework material with open Ag + sites. *Environ. Sci. Technol.* **51**, 3471–3479 (2017).
26. Amendola, V., Bergamaschi, G., Boiocchi, M., Alberto, R. & Braband, H. Fluorescent sensing of Tc-99 pertechnetate in water. *Chem. Sci.* **5**, 1820–1826 (2014).
27. Cornes, S. P., Sambrook, M. R. & Beer, P. D. Selective perrhenate recognition in pure water by halogen bonding and hydrogen bonding alpha-cyclodextrin based receptors. *Chem. Commun.* **53**, 3866–3869 (2017).
28. Ravi, A. et al. Finding a receptor design for selective recognition of perrhenate and pertechnetate: hydrogen vs. halogen bonding. *Chem. Commun.* **54**, 4826–4829 (2018).
29. Kataev, E. A. et al. Perrhenate and pertechnetate anion recognition properties of cyclo[8]pyrrole. *Supramol. Chem.* **27**, 346–356 (2015).
30. Alberti, G. et al. Supramolecular receptors in solid phase: developing sensors for anionic radionuclides. *Dalton Trans.* **42**, 6227–6234 (2013).
31. Ji, X. F. et al. Physical removal of anions from aqueous media by means of a macrocycle-containing polymeric network. *J. Am. Chem. Soc.* **140**, 2777–2780 (2018).
32. Jung, O. S., Kim, Y. J., Lee, Y. A., Park, J. K. & Chae, H. K. Smart molecular helical springs as tunable receptors. *J. Am. Chem. Soc.* **122**, 9921–9925 (2000).
33. Kitagawa, S. & Uemura, K. Dynamic porous properties of coordination polymers inspired by hydrogen bonds. *Chem. Soc. Rev.* **34**, 109–119 (2005).
34. Horike, S., Shimomura, S. & Kitagawa, S. Soft porous crystals. *Nat. Chem.* **1**, 695–704 (2009).
35. Vanduyfhuys, L. et al. Thermodynamic insight into stimuli-responsive behaviour of soft porous crystals. *Nat. Commun.* **9**, 204 (2018).
36. Jie, K. C., Zhou, Y. J., Li, E. R. & Huang, F. H. Nonporous adaptive crystals of pillararenes. *Acc. Chem. Res.* **51**, 2064–2072 (2018).
37. Lehn, J. M. Toward complex matter: Supramolecular chemistry and self-organization. *Proc. Natl Acad. Sci. USA* **99**, 4763–4768 (2002).
38. Aida, T., Meijer, E. W. & Stupp, S. I. Functional supramolecular polymers. *Science* **335**, 813–817 (2012).
39. Kaabel, S. et al. Chiral hemicucurbit[8]uril as an anion receptor: selectivity to size, shape and charge distribution. *Chem. Sci.* **8**, 2184–2190 (2017).
40. Yawer, M. A., Havel, V. & Sindelar, V. A bambusuril macrocycle that binds anions in water with high affinity and selectivity. *Angew. Chem. Int. Ed.* **54**, 276–279 (2015).
41. Svec, J., Necas, M. & Sindelar, V. Bambus[6]uril. *Angew. Chem. Int. Ed.* **49**, 2378–2381 (2010).
42. Zhang, M. L., Lin, R. L., Sun, W. Q. & Liu, J. X. Anion encapsulation and complexation by cucurbit[n]urils and their derivatives. *J. Incl. Phenom. Macro.* **90**, 173–187 (2018).
43. Ni, X. L. et al. Self-assemblies based on the "outer-surface interactions" of cucurbit[n]urils: new opportunities for supramolecular architectures and materials. *Acc. Chem. Res.* **47**, 1386–1395 (2014).
44. Chen, K. et al. Cucurbit[6]uril-based supramolecular assemblies: possible application in radioactive cesium cation capture. *J. Am. Chem. Soc.* **136**, 16744–16747 (2014).
45. Liu, L., Jiang, X. A. & Zhang, J. Anion-linked cucurbit[6]uril frameworks formed by microwave-assisted synthesis in ionic liquids. *CrystEngcomm* **12**, 3445–3447 (2010).
46. Barrow, S. J., Kasera, S., Rowland, M. J., del Barrio, J. & Scherman, O. A. Cucurbituril-based molecular recognition. *Chem. Rev.* **115**, 12320–12406 (2015).
47. Ko, Y. H., Kim, E., Hwang, I. & Kim, K. Supramolecular assemblies built with host-stabilized charge-transfer interactions. *Chem. Commun.* **13**, 1305–1315 (2007).
48. Kim, H. J. et al. Selective inclusion of a hetero-guest pair in a molecular host: Formation of stable charge-transfer complexes in cucurbit[8]uril. *Angew. Chem. Int. Ed.* **40**, 1526–1529 (2001).
49. Tian, J., Wang, H., Zhang, D. W., Liu, Y. & Li, Z. T. Supramolecular organic frameworks (SOFs): homogeneous regular 2D and 3D pores in water. *Natl. Sci. Rev.* **4**, 426–436 (2017).
50. Tian, J. et al. Supramolecular metal-organic frameworks that display high homogeneous and heterogeneous photocatalytic activity for H-2 production. *Nat. Commun.* **7**, 11580 (2016).
51. Tian, J. et al. Three-dimensional periodic supramolecular organic framework ion sponge in water and microcrystals. *Nat. Commun.* **5**, 5574 (2014).
52. Kim, K. et al. Functionalized cucurbiturils and their applications. *Chem. Soc. Rev.* **36**, 267–279 (2007).
53. Mitkina, T. V., Naumov, D. Y., Kurat'eva, N. V., Gerasko, O. A. & Fedin, V. P. Synthesis and guest exchange reactions of inclusion compounds of cucurbit[8] uril with nickel(II) and copper(II) complexes. *Russ. Chem. Bull.* **55**, 26–35 (2006).
54. Biedermann, F., Uzunova, V. D., Scherman, O. A., Nau, W. M. & De Simone, A. Release of high-energy water as an essential driving force for the high-affinity binding of cucurbit[n]urils. *J. Am. Chem. Soc.* **134**, 15318–15323 (2012).
55. Biedermann, F., Vendruscolo, M., Scherman, O. A., De Simone, A. & Nau, W. M. Cucurbit[8]uril and blue-box: high-energy water release overwhelms electrostatic interactions. *J. Am. Chem. Soc.* **135**, 14879–14888 (2013).
56. Banerjee, D. et al. Removal of pertechnetate-related oxyanions from solution using functionalized hierarchical porous frameworks. *Chem. Eur. J.* **22**, 17581–17584 (2016).
57. Li, J. et al. $^{99}TcO_4^-$ remediation by a cationic polymeric network. *Nat. Commun.* **9**, 3007 (2018).
58. Zhu, L. et al. Exceptional perrhenate/pertechnetate uptake and subsequent immobilization by a low-dimensional cationic coordination. *Polym.: Overcoming Hofmeister Bias Sel. Environ. Sci. Tech. Let.* **4**, 316–322 (2017).
59. Perdew, J. P., Burke, K. & Ernzerhof, M. Generalized gradient approximation made simple. *Phys. Rev. Lett.* **77**, 3865–3868 (1996).
60. Kresse, G. & Furthmuller, J. Efficient iterative schemes for ab initio total-energy calculations using a plane-wave basis set. *Phys. Rev. B* **54**, 11169–11186 (1996).
61. Koch, U. & Popelier, P. L. A. Characterization of C-H-O hydrogen-bonds on the basis of the charge-density. *J. Phys. Chem.* **99**, 9747–9754 (1995).
62. Espinosa, E., Souhassou, M., Lachekar, H. & Lecomte, C. Topological analysis of the electron density in hydrogen bonds. *Acta Crystallogr. B.* **55**, 563–572 (1999).
63. Espinosa, E., Alkorta, I., Elguero, J. & Molins, E. From weak to strong interactions: a comprehensive analysis of the topological and energetic properties of the electron density distribution involving X-H center dot center dot center dot F-Y systems. *J. Chem. Phys.* **117**, 5529–5542 (2002).
64. Lefebvre, C. et al. Accurately extracting the signature of intermolecular interactions present in the NCI plot of the reduced density gradient versus electron density. *Phys. Chem. Chem. Phys.* **19**, 17928–17936 (2017).
65. Johnson, E. R. et al. Revealing noncovalent interactions. *J. Am. Chem. Soc.* **132**, 6498–6506 (2010).
66. Day, A., Arnold, A. P., Blanch, R. J. & Snushall, B. Controlling factors in the synthesis of cucurbituril and its homologues. *J. Org. Chem.* **66**, 8094–8100 (2001).
67. Sheldrick, G. M. A short history of SHELX. *Acta Crystallogr. A* **64**, 112–122 (2008).
68. Sheldrick, G. M. SHELXT—integrated space-group and crystal-structure determination. *Acta Crystallogr. A* **71**, 3–8 (2015).

Acknowledgements

We thank the support from the National Natural Science Foundation of China (21671191 and 11405186) and the Major Program of National Natural Science Foundation of China (21790373). The Science Challenge Project (TZ2016004) is also acknowledged. J.G. was supported by the Center for Actinide Science and Technology, an Energy Frontier Research Center funded by the U.S. Department of Energy under Award DE-SC0016568.

Author contributions

W.Q.S. conceived and supervised the project. L.M. designed and synthesized the material. L.M. and F.Z.L. carried out the uptake experiments and analyzed the data. C.X., H.D., and J.C. performed the Tc-99 experiments. L.M. and K.Q.H. collected and analyzed the crystal data. L.W. performed the TEM-EDS analysis. J.H.L., C.Z.W., and Q.Y.W. performed the modeling and theoretical calculations. L.M., F.Z.L., J.H.L., C.Z.W., and Q.Y. W. wrote the paper. W.Q.S., Z.F.C., and J.K.G. reviewed and edited the paper. All authors discussed the results and commented on the manuscript.

Additional information

Supplementary Information accompanies this paper at https://doi.org/10.1038/s41467-019-09504-3.

Competing interests: The authors declare no competing interests.

Reprints and permission information is available online at http://npg.nature.com/reprintsandpermissions/

Journal peer review information: *Nature Communications* thanks Valeria Amendola and the other anonymous reviewer(s) for their contribution to the peer review of this work.

Publisher's note: Springer Nature remains neutral with regard to jurisdictional claims in published maps and institutional affiliations.